Measurement of the time spent by a tunnelling atom within the barrier region

https://doi.org/10.1038/s41586-020-2490-7

Received: 31 July 2019

Accepted: 27 April 2020

Published online: 22 July 2020

Check for updates

Ramón Ramos[1,3]✉, David Spierings[1], Isabelle Racicot[1] & Aephraim M. Steinberg[1,2]

Tunnelling is one of the most characteristic phenomena of quantum physics, underlying processes such as photosynthesis and nuclear fusion, as well as devices ranging from superconducting quantum interference device (SQUID) magnetometers to superconducting qubits for quantum computers. The question of how long a particle takes to tunnel through a barrier, however, has remained contentious since the first attempts to calculate it[1]. It is now well understood that the group delay[2]—the arrival time of the peak of the transmitted wavepacket at the far side of the barrier—can be smaller than the barrier thickness divided by the speed of light, without violating causality. This has been confirmed by many experiments[3–6], and a recent work even claims that tunnelling may take no time at all[7]. There have also been efforts to identify a different timescale that would better describe how long a given particle spends in the barrier region[8–10]. Here we directly measure such a time by studying Bose-condensed ^{87}Rb atoms tunnelling through a 1.3-micrometre-thick optical barrier. By localizing a pseudo-magnetic field inside the barrier, we use the spin precession of the atoms as a clock to measure the time that they require to cross the classically forbidden region. We study the dependence of the traversal time on the incident energy, finding a value of 0.61(7) milliseconds at the lowest energy for which tunnelling is observable. This experiment lays the groundwork for addressing fundamental questions about history in quantum mechanics: for instance, what we can learn about where a particle was at earlier times by observing where it is now[11–13].

The earliest attempts to calculate the time a tunnelling particle spends in the barrier region (not to be confused with the lifetime of a quasi-bound state) addressed the propagation delay for a wavepacket peak; however, work in the 1980s, particularly by Büttiker and Landauer[14,15], shifted the discussion to an 'interaction time', the time actually spent by a particle in the barrier. This was motivated by the prediction[16] that in certain regimes, the wavepacket delay (sometimes referred to as the 'phase time' or 'Wigner time'[2]) could appear to be superluminal, suggesting that it does not reflect the duration of the tunnelling event. Büttiker and Landauer provided arguments in favour of a 'semiclassical time' equal to $md/\hbar\kappa$, where m is the mass of the particle, d is the barrier thickness and $\kappa = \sqrt{2m(V_0 - E)}/\hbar$ is the evanescent decay constant in the tunnelling regime (E is the incident energy, V_0 is the barrier height and $\hbar$ is the reduced Planck constant); it should be noted that unlike the group delay, this grows linearly with d and is therefore generally not superluminal. As we shall discuss in depth below, another way of defining the tunnelling duration is via the effect a particle has on a degree of freedom that acts as an auxiliary 'clock'.

A number of experiments have sought to measure tunnelling times. Several experiments[3–6] have confirmed the superluminal nature of the group delay, and some have attempted to probe other timescales—including the Larmor times we focus on in this paper—using analogue optical systems[17,18] and an elegant neutron experiment[19], although the latter was for a very different propagation problem. A pioneering experiment studying quantum tunnelling in a Josephson junction[20] was the first attempt to apply the insights of Büttiker and Landauer to instead probe the duration of the tunnelling event itself; the experiment offered qualitative agreement with the 'semiclassical time'.

Recently, there has been increased experimental interest in the area owing to the development of the 'attoclock'[21]. These experiments[7,22–26] use strong-field ionization in an elliptically polarized field to determine how much time elapses between the ionizing field reaching its maximum and an electron finally escaping. Intuitively, one might therefore expect such times to be related to a wavepacket delay (as opposed to a 'dwell' or interaction time), although there have been multiple theoretical approaches[26–28] and no small amount of controversy. In the attoclock experiments, instead of impinging upon a barrier, the electron escapes from a quasi-bound state (note the distinction made early on between escape time and traversal time)[29]. Therefore, it is impossible to identify a time at which the event 'starts', as opposed to merely the moment at which the field reaches its maximum. The problem is further complicated by electron–electron correlation and atomic-physics effects, which generate additional delays unrelated to the tunnelling event[28]. The most recent work, which eliminated some of these effects by carrying out the experiment in hydrogen, made the claim that tunnelling is essentially instantaneous[7]. There has also been an experiment probing the time delay between two tunnel-coupled momentum components

[1]Centre for Quantum Information and Quantum Control and Institute for Optical Sciences, Department of Physics, University of Toronto, Toronto, Ontario, Canada. [2]Canadian Institute For Advanced Research, Toronto, Ontario, Canada. [3]Present address: ICFO – Institut de Ciències Fotòniques, Barcelona, Spain. ✉e-mail: jramonra@physics.utoronto.ca

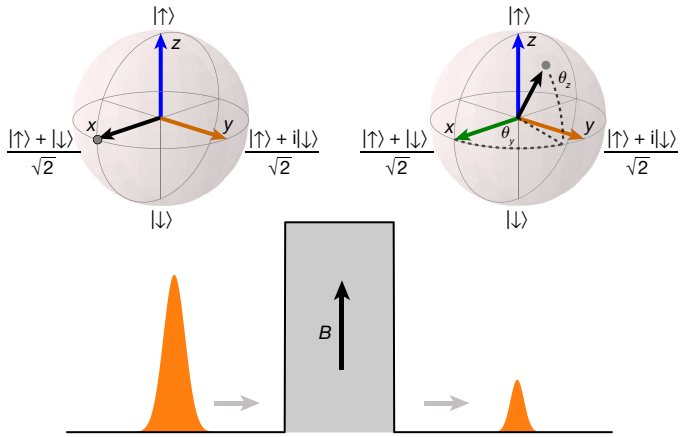

Fig. 1 | Larmor clock. A weak magnetic field B pointing in the z direction is localized inside the potential barrier. A particle with spin-½ pointing initially along the x direction impinges on the barrier, and after transmission, the spin has precessed in the x–y plane with a Larmor frequency ω_L and tilted towards the z axis, as depicted in the Bloch sphere. The $|\uparrow\rangle$ and $|\downarrow\rangle$ states are the eigenstates of the system in the presence of the magnetic field along the z axis. The Larmor times are then defined as $\tau_y = \theta_y/\omega_L$ and $\tau_z = \theta_z/\omega_L$.

of atoms oscillating in the wells of an optical lattice[30], although it was unable to discriminate between the different theories.

To provide an operational definition of the tunnelling time, it is natural to devise a 'clock' which ticks only while the particle is present in the barrier region. The Larmor clock[15,31,32] is the most famous example of such a thought experiment. If an ensemble of polarized spin-½ particles impinges on a barrier, localizing a magnetic field in the barrier region alone will cause the spins to precess only while the particles are under the barrier (Fig. 1). Considering incident particles polarized in the x direction and a magnetic field along z, one would expect the spin to precess by an angle $\theta = \omega_L\tau$, where ω_L is the Larmor frequency and τ is the time spent in the barrier. By working in the limit of a weak magnetic field ($\omega_L \to 0$), this time can be measured without substantially perturbing the tunnelling particle. Büttiker[15] noted that even in this limit, measurement back-action cannot be neglected, and it results in preferential transmission of atoms aligned with the magnetic field. This leads to two spin rotation angles: a precession in the plane orthogonal to the applied magnetic field, θ_y, as well as an alignment along the direction of the field, θ_z. He defined times associated with the spin projections: τ_z, τ_y and $\tau_x = \sqrt{\tau_y^2 + \tau_z^2}$; the latter is often known as the 'Büttiker time'. It turns out that combinations of two such quantities appear in other theoretical treatments as a single complex number[33,34], but researchers were hesitant to accept complex-valued times without a clear interpretation. Later, further studies[11,12] associated τ_y and τ_z with the real and imaginary parts of the 'weak value'[13] of a dwell-time operator, thereby providing them with distinct interpretations as the inherent tunnelling time and the measurement back-action, respectively.

We have built an experiment to implement the Larmor clock, making use of the long de Broglie wavelengths achievable in atomic Bose–Einstein condensates and the remarkable degree of control possible in such systems, both for tailoring optical potentials and for manipulating and measuring spins. The spatial resolution of the potentials is limited only by the wavelength of the laser light used, and at our energy scales—which are of the order of $E \approx 100$ feV ($k_B \times 1$ nK, where k_B is the Boltzmann constant)—the tunnelling probability is sizeable, and the millisecond-level timescales are convenient to probe experimentally. We map the proposed Larmor clock to our experiment by creating a pseudo spin-½ system using two of the hyperfine states in our system. We couple these states through a two-photon Raman transition, driven by the barrier beam itself, thus generating a pseudo-magnetic field for the Larmor clock implementation: the effective Larmor frequency ω_L is set by the two-photon Rabi frequency Ω. Using this scheme, we are able to determine the barrier traversal time in our system by measuring the final spin state of the transmitted atoms.

We prepare a degenerate gas of approximately 8,000 ^{87}Rb atoms in the $5S_{1/2}|F = 2, m_F = 2\rangle$ state (F and m_F denote the hyperfine and Zeeman quantum numbers, respectively) in a crossed dipole trap. One of the trap beams is turned off and the atoms are left free to move longitudinally in a quasi one-dimensional waveguide. We decrease the effective temperature of the atoms using matter-wave lensing (see Methods), resulting in a root mean square (r.m.s.) velocity spread of 0.45(15) mm s^{-1}, or an equivalent effective temperature of 2(1) nK (de Broglie wavelength, $\lambda_{dB} = 4(1)$ μm). We then push the atoms towards a 1.3-μm Gaussian barrier, that is formed by a focused blue-detuned laser beam (see Methods), by exploiting the magnetic moment of the atoms and momentarily accelerating them using a magnetic gradient pulse to set the velocity. We have previously observed tunnelling through this potential in two different contexts: escape from a quasi-bound state[35,36] and in a single-collision geometry[37] that is similar to that studied here. While the atoms approach the potential barrier, rapid adiabatic passage is used to transfer the atoms from their initial spin state to the $|2, 0\rangle$ state. An effective spin-½ is encoded in the $|2, 0\rangle$ and $|1, 0\rangle$ hyperfine clock states denoted by $|+x\rangle = (|\uparrow\rangle + |\downarrow\rangle)/\sqrt{2}$ and $|-x\rangle = (|\uparrow\rangle - |\downarrow\rangle)/\sqrt{2}$, respectively (Fig. 2). The barrier light is phase-modulated at the 6.8-GHz

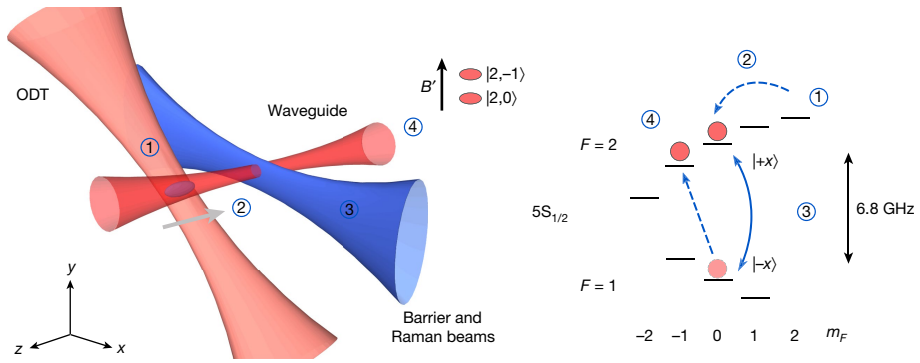

Fig. 2 | Experimental setup and sequence. We create a Bose–Einstein condensate in the $|F = 2, m_F = 2\rangle$ state in a crossed dipole trap formed by an optical waveguide and an intersecting perpendicular beam (ODT). Left, experimental setup; right, atomic-level scheme. (1) After the effective temperature of the cloud is lowered, the atoms are pushed by a pulsed magnetic field gradient along the waveguide in the $-z$ direction towards a blue-detuned beam that generates the potential barrier and the pair of Raman beams. (2) While the atoms travel towards the barrier, we use rapid adiabatic passage to transfer them to the $|2, 0\rangle$ ($|+x\rangle$) state. (3) During the interaction with the barrier, the pair of Raman beams couples the $|+x\rangle$ and $|-x\rangle$ states separated by the 6.8-GHz hyperfine splitting. (4) To perform the read-out sequence, the atoms that were coupled to $|-x\rangle$ are transferred to the $|2, -1\rangle$ state, after which we apply a magnetic field gradient B' to perform a Stern–Gerlach measurement and separately image both of the states.

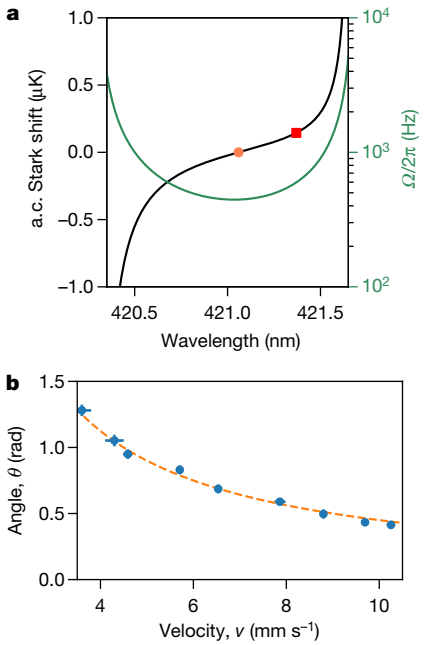

Fig. 3 | Implementation of the Larmor clock. a, Scalar a.c. Stark shift (black line) created by the tunable laser beam used for the optical potential. The two points represent the wavelengths used in the experiment: the orange dot is the wavelength at which the barrier height vanishes (tune-out wavelength) and where the free-space Larmor measurement is performed, and the red square is the wavelength used to create a 135-nK potential barrier. The pair of Raman beams, with two-photon Rabi frequency indicated by the green line, is created with the same beam as the barrier. **b**, Measurement of the precession angle at the tune-out wavelength. The error bars represent the standard error of the mean and are mostly smaller than the symbol size. The dashed line is a one-parameter fit to the expression $\Omega d/v$, where d is the effective barrier width, v is the incident velocity of the atoms and Ω is the Rabi frequency, which is left as a free parameter. We find $\Omega = 2\pi \times 440(10)$ Hz. Ω can be controlled independently of the barrier height and was reduced for the tunnelling data (see Methods).

hyperfine frequency, thus creating a pair of Raman beams that couple the $|+x\rangle$ and $|-x\rangle$ states. In the interaction picture, the pseudo-magnetic field generated by the Raman beams points along the z direction of the Bloch sphere. After the collision with the barrier is complete, we perform a final rapid adiabatic passage sweep from $|-x\rangle$ to $|2, -1\rangle$. A subsequent Stern–Gerlach sequence separates the two spin states, enabling us to determine the populations of $|\pm x\rangle$.

We begin by testing the implementation of the Larmor clock in free space. For this purpose, we remove the potential barrier but keep the pseudo-magnetic field on by changing the barrier wavelength to a nearby tune-out wavelength (see Fig. 3 and Methods). The precession angle tells us how much time the atoms spend in the region with the localized pseudo-magnetic field. The results without the barrier (Fig. 3b) show an expected $1/v$ dependence, where v is the velocity of the atoms. With our knowledge of the barrier width, we can extract the Rabi frequency of the two-photon transition.

After verifying the behaviour of the clock, we move to the case of a repulsive barrier. In this case, after the interaction with the barrier and the Raman beams, each atom will be either transmitted or reflected, with its spin in a superposition of the $|+x\rangle$ and $|-x\rangle$ states (Fig. 4a). At high energies, the barrier has little effect on the atoms and the semiclassical treatment is a good approximation; we therefore deduce the Rabi frequency from the high-energy measurements (see Methods). We perform the tunnelling measurement with a barrier height of 135(8) nK, corresponding to 5.1 mm s^{-1} and a Rabi frequency of $\Omega = 2\pi \times 225(40)$ Hz.

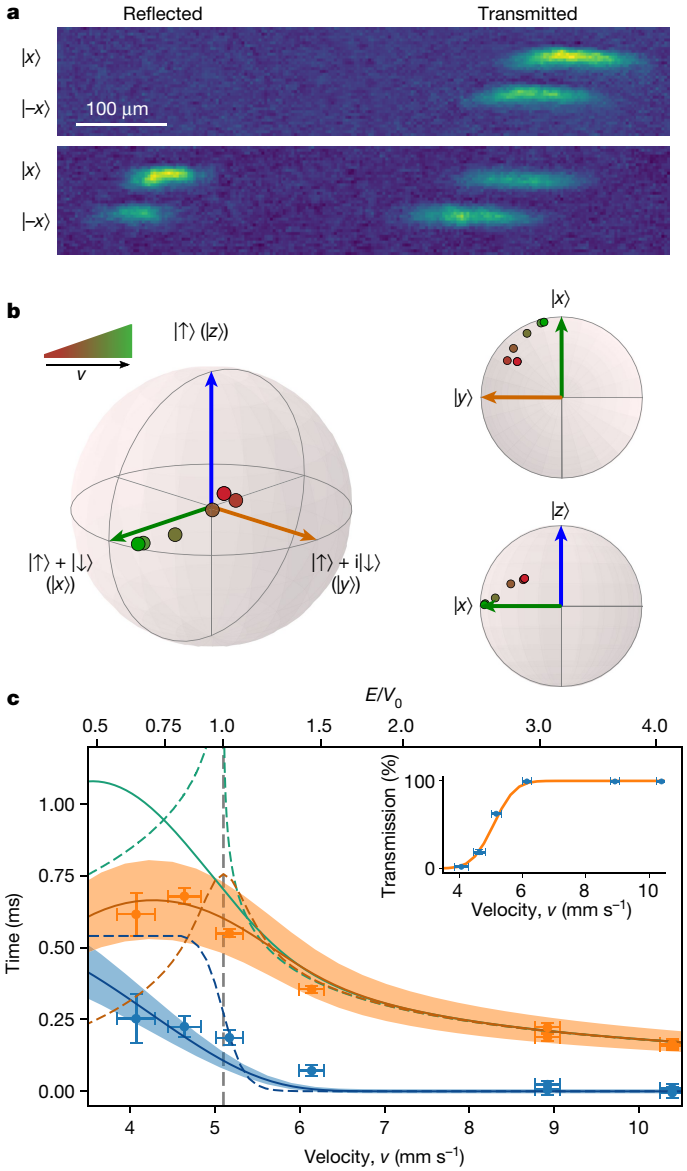

Fig. 4 | Traversal time of an atomic wavepacket through an optical potential. a, Absorption images of the atomic densities after the interaction with a 135-nK barrier and the Raman beams for incident energies of 400 nK (top) and 140 nK (bottom). A Stern–Gerlach pulse is used to separate the two spin components; a nearly 45° angle exists between the magnetic field gradient and the propagation direction. The precession angles for the transmitted atoms are obtained by doing full tomography on the spin-½ system. **b**, Obtained spin projections for the different incident velocities. The top right and bottom right figures show cuts along the x–y and x–z planes. The data are colour-coded to indicate velocity (red, lower velocities; green, higher velocities). **c**, Experimental data of the Larmor times τ_y (orange dots) and τ_z (blue dots) as a function of incident velocity. The error bars denote the standard error of the mean and in some cases are smaller than the symbol size. The dashed grey line corresponds to the velocity matching the height of the barrier (5.1 mm s^{-1}). Light orange and blue regions are the one-dimensional two-component time-dependent Schrödinger simulations, and the bands represent one standard deviation on the measured Rabi frequency. The dashed lines are monochromatic weak-measurement theory predictions for the Larmor times τ_y (orange) and τ_z (blue), and the semiclassical time (green). The corresponding solid lines are calculated by taking into account the velocity spread of the initial wavepacket (0.45 mm s^{-1}). Inset, transmission-probability data (blue dots) and two-component time-dependent Schrödinger simulations using a wavepacket with a velocity spread of 0.45 mm s^{-1} (orange line).

We investigate the two Larmor times by performing full-spin tomography of the transmitted spin-½ particles. Rotations after the scattering event enable us to measure the spin components along the x, y and z axes of the Bloch sphere (Fig. 4b). From the different projections, we find the traversal time τ_y and the time τ_z associated with the back-action of the measurement (Fig. 4c). At the lowest incident velocity (4.1 mm s^{-1}), we observe a transmission probability of 3%. Given the energy dependence of the transmission, we calculate that the transmitted atoms have a velocity distribution with a peak at 4.8 mm s^{-1}, corresponding to $\kappa d \approx 3$. About three-quarters of this distribution corresponds to energies below the barrier height. The measured traversal time τ_y is 0.61(7) ms.

The experimental data are in good agreement with one-dimensional two-component time-dependent Schrödinger simulations with no free parameters (Fig. 4c), and Gross–Pitaevskii simulations show no sizeable modifications from the presence of interactions. Furthermore, the theoretical prediction given by the weak value formalism describes our results well (see Methods). By contrast, the 'semiclassical time' disagrees with τ_x by more than three standard deviations for the lowest velocities.

This is, to our knowledge, the first direct measurement of the time that massive particles spend in a barrier region, and successfully implements the Larmor clock thought experiment. For a range of incident velocities, we can observe both the time spent in the barrier and also the spin rotation owing to measurement back-action, clearly separating the two effects. We see that as we head deeper into the quantum regime, the back-action grows in importance, and our results are consistent with the prediction that the tunnelling time begins to decrease[15]. Our results are inconsistent with claims that tunnelling takes 'zero time'[7,22]. Beyond resolving the controversy regarding how long a tunnelling particle spends in the barrier region, the experimental approach we demonstrate here opens a window on quantum measurement and the broad question of how much can be inferred about the history of a quantum particle. In particular, it will enable measurements of at what position within a barrier the transmitted and reflected particles spend their time[11,12]. As it is predicted that such measurements exhibit non-classical behaviour, their study as the system is made 'more classical' by the introduction of dissipation or atomic interactions promises to offer new perspectives on the quantum–classical boundary.

Online content

Any methods, additional references, Nature Research reporting summaries, source data, extended data, supplementary information, acknowledgements, peer review information; details of author contributions and competing interests; and statements of data and code availability are available at https://doi.org/10.1038/s41586-020-2490-7.

1. MacColl, L. A. Note on the transmission and reflection of wave packets by potential barriers. *Phys. Rev.* **40**, 621–626 (1932).
2. Wigner, E. P. Lower limit for the energy derivative of the scattering phase shift. *Phys. Rev.* **98**, 145–147 (1955).
3. Ranfagni, A., Mugnai, D., Fabeni, P. & Pazzi, G. P. Delay-time measurements in narrowed waveguides as a test of tunneling. *Appl. Phys. Lett.* **58**, 774–776 (1991).
4. Enders, A. & Nimtz, G. On superluminal barrier traversal. *J. Phys. I* **2**, 1693–1698 (1992).
5. Steinberg, A. M., Kwiat, P. G. & Chiao, R. Y. Measurement of the single-photon tunneling time. *Phys. Rev. Lett.* **71**, 708–711 (1993).
6. Spielmann, C., Szipöcs, R., Stingl, A. & Krausz, F. Tunneling of optical pulses through photonic band gaps. *Phys. Rev. Lett.* **73**, 2308–2311 (1994).
7. Sainadh, U. S. et al. Attosecond angular streaking and tunnelling time in atomic hydrogen. *Nature* **568**, 75–77 (2019).
8. Hauge, E. H. & Støvneng, J. A. Tunneling times: a critical review. *Rev. Mod. Phys.* **61**, 917–936 (1989).
9. Landauer, R. & Martin, T. Barrier interaction time in tunneling. *Rev. Mod. Phys.* **66**, 217–228 (1994).
10. Chiao, R. Y. & Steinberg, A. M. in *Progress in Optics* Vol. 37 (ed. Wolf, E.) 345–405 (Elsevier, 1997).
11. Steinberg, A. M. How much time does a tunneling particle spend in the barrier region? *Phys. Rev. Lett.* **74**, 2405–2409 (1995).
12. Steinberg, A. M. Conditional probabilities in quantum theory and the tunneling-time controversy. *Phys. Rev. A* **52**, 32–42 (1995).
13. Aharonov, Y. & Vaidman, L. How the result of a measurement of a component of the spin of a spin-½ particle can turn out to be 100. *Phys. Rev. Lett.* **60**, 1351–1354 (1988).
14. Büttiker, M. & Landauer, R. Traversal time for tunneling. *Phys. Rev. Lett.* **49**, 1739–1742 (1982).
15. Büttiker, M. Larmor precession and the traversal time for tunneling. *Phys. Rev. B* **27**, 6178–6188 (1983).
16. Hartman, T. E. Tunneling of a wave packet. *J. Appl. Phys.* **33**, 3427–3433 (1962).
17. Deutsch, M. & Golub, J. Optical Larmor clock: measurement of the photonic tunneling time. *Phys. Rev. A* **53**, 434–439 (1996).
18. Balcou, P. & Dutriaux, L. Dual optical tunneling times in frustrated total internal reflection. *Phys. Rev. Lett.* **78**, 851–854 (1997).
19. Hino, M. et al. Measurement of Larmor precession angles of tunneling neutrons. *Phys. Rev. A* **59**, 2261–2268 (1999).
20. Esteve, D. et al. Observation of the temporal decoupling effect on the macroscopic quantum tunneling of a Josephson junction. In *Proc. 9th Gen. Conf. Condensed Matter Division of the European Physical Society* (eds Friedel, J. et al.) 121–124 (1989).
21. Eckle, P. et al. Attosecond angular streaking. *Nat. Phys.* **4**, 565–570 (2008).
22. Eckle, P. et al. Attosecond ionization and tunneling delay time measurements in helium. *Science* **322**, 1525–1529 (2008).
23. Pfeiffer, A. N., Cirelli, C., Smolarski, M. & Keller, U. Recent attoclock measurements of strong field ionization. *Chem. Phys.* **414**, 84–91 (2013).
24. Landsman, A. S. et al. Ultrafast resolution of tunneling delay time. *Optica* **1**, 343–349 (2014).
25. Camus, N. et al. Experimental evidence for quantum tunneling time. *Phys. Rev. Lett.* **119**, 023201 (2017).
26. Zimmermann, T., Mishra, S., Doran, B. R., Gordon, D. F. & Landsman, A. S. Tunneling time and weak measurement in strong field ionization. *Phys. Rev. Lett.* **116**, 233603 (2016).
27. Klaiber, M., Hatsagortsyan, K. Z. & Keitel, C. H. Under-the-tunneling-barrier recollisions in strong-field Ionization. *Phys. Rev. Lett.* **120**, 013201 (2018).
28. Torlina, L. et al. Interpreting attoclock measurements of tunnelling times. *Nat. Phys.* **11**, 503–508 (2015).
29. Landauer, R. Barrier traversal time. *Nature* **341**, 567–568 (1989).
30. Fortun, A. et al. Direct tunneling delay time measurement in an optical lattice. *Phys. Rev. Lett.* **117**, 010401 (2016).
31. Baz', A. I. Lifetime of intermediate states. *Sov. J. Nucl. Phys.* **4**, 182–188 (1966).
32. Rybachenko, V. F. Time of penetration of a particle through a potential barrier. *Sov. J. Nucl. Phys.* **5**, 635–639 (1967).
33. Pollak, E. & Miller, W. H. New physical interpretation for time in scattering theory. *Phys. Rev. Lett.* **53**, 115–118 (1984).
34. Sokolovski, D. & Baskin, L. M. Traversal time in quantum scattering. *Phys. Rev. A* **36**, 4604–4611 (1987).
35. Potnis, S., Ramos, R., Maeda, K., Carr, L. D. & Steinberg, A. M. Interaction-assisted quantum tunneling of a Bose–Einstein condensate out of a single trapping well. *Phys. Rev. Lett.* **118**, 060402 (2017).
36. Zhao, X. et al. Macroscopic quantum tunneling escape of Bose–Einstein condensates. *Phys. Rev. A* **96**, 063601 (2017).
37. Ramos, R., Spierings, D., Potnis, S. & Steinberg, A. M. Atom-optics knife edge: measuring narrow momentum distributions. *Phys. Rev. A* **98**, 023611 (2018).

Methods

Experimental setup

We Bose-condense 8,000 ^{87}Rb atoms in a 1,064-nm crossed dipole trap. The trap is composed of two beams: an elongated beam that we refer to as the atom waveguide (with a waist of 15 μm and a Rayleigh range of $z_0 \approx 600$ μm), and an orthogonal beam intersecting the waveguide nearly 150 μm away from its centre. The atoms start at the intersection of the two beams. The atom waveguide has radial and longitudinal frequencies of $\nu_r = 220$ Hz and $\nu_l = 2.7$ Hz. The barrier beam, formed by a 421-nm laser focused to 1.3 μm (see below), intersects the waveguide close to its centre. The longitudinal trap frequency sets the minimum velocity at which the atoms meet the barrier, as the waveguide curvature produces an acceleration of 5×10^{-2} m s^{-2}.

Matter-wave lensing

We use delta-kick cooling[38–42], also referred to as matter-wave lensing, to decrease the effective temperature of the atoms from 15 nK to 2(1) nK, corresponding to an r.m.s. velocity spread of 0.45(15) mm s^{-1}. The effective temperature is given by $T_{\mathrm{eff}} = m\Delta v^2/k_B$ where Δv is the r.m.s. width of the atomic velocity distribution, m is the atomic mass and k_B is the Boltzmann constant. After cooling, the atoms have a thermal de Broglie wavelength of $\lambda_{\mathrm{dB}} = 4(1)$ μm. The cooling procedure is as follows: the atoms start in a crossed dipole trap, then are released from one of these beams (ODT) and expand in the atom waveguide for 9 ms (to approximately four times the initial cloud size), and then a quasi-harmonic trap with a frequency of $\omega = 2\pi \times 50(5)$ Hz, created by the ODT beam, is flashed for 1.1 ms to collimate the atomic wavepacket. The amount of expansion is limited by the radius of the beam ($1/e^2$ radius of 100 μm); this expansion time is kept short enough that the atoms remain within the harmonic region of the Gaussian potential. The condensate has a final longitudinal r.m.s. radius of 15 μm. By reducing the initial number of atoms we have achieved temperatures as low as 0.9 nK using this technique, but to work at higher atom numbers we perform this experiment at 2 nK.

Potential barrier and Raman beams

The light for the barrier and the Raman beams is created by a custom-made 421-nm external cavity diode laser (ECDL) in Littrow configuration. We set the frequency of this beam in the vicinity of one of the rubidium tune-out wavelengths (421.07 nm) located between the $5S_{1/2} \rightarrow 6P_{1/2}$ (421.7 nm) and the $5S_{1/2} \rightarrow 6P_{3/2}$ (420.3 nm) transitions. To generate the pair of Raman beams, the beam passes through a 6.8-GHz electro-optic phase modulator using a modulation depth of $\beta \approx 0.3$, which creates a pair of sidebands in the optical spectrum. About 5% of the optical power goes to the sidebands. The generated sidebands have opposite phases and act destructively when used along with the carrier to drive Raman transitions. An etalon with a full width at half-maximum bandwidth of 12 GHz is therefore used to remove one of the sidebands. We can control the Rabi frequency without modifying the power of the Raman beams by adjusting the modulation depth, β. This is monitored by detecting the beat signal between the carrier and the remaining sideband on a fast photodiode.

The barrier light is sent to the science chamber, where it is focused to a $1/e^2$ radius of $w_z = 1.3$ μm along the z direction, and along the y direction it is scanned with an acousto-optical deflector to create a flat, 50-μm-wide potential. The scan rate of the potential (133 kHz) is faster than any atomic dynamics and guarantees that the cloud experiences a time-averaged potential. The Rayleigh range of the beam is 8 μm, larger than the transverse radius of the condensate (~2.5 μm). We can set the wavelength to 421.38 nm, where a power of approximately 0.5 mW generates a repulsive potential as large as $V_0/k_B \approx 180$ nK (given, for the $m_F = 0$ clock states, by the scalar a.c. Stark shift)[43]. A magnetic field pointing along the propagation axis of the beams (x direction) sets the quantization axis. The beams are circularly polarized to drive σ^+–σ^+ Raman transitions.

To calibrate the Rabi frequency, we study high-velocity incident atoms traversing the barrier. For these velocities, the semiclassical approximation is valid (see Fig. 4), and the calibration can be obtained from $\theta = \Omega \int_{-\infty}^{\infty} G(z)\mathrm{d}z/\sqrt{v^2 - v_b^2 G(z)}$, where $G(z) = \exp(-2z^2/w_z^2)$ is the Gaussian envelope of the potential, v is the velocity of the atoms and v_b is the velocity corresponding to the barrier height. The Rabi frequency can also be calibrated at the tune-out wavelength. Accounting for the difference in a.c. Stark shift between the barrier and tune-out wavelengths, and frequency-dependent transmission owing to etaloning effects in our chamber windows, the two techniques differ by about 10%. However, owing to the limited tunability of the barrier ECDL, we use the first method to calibrate the Rabi frequency.

Calculations of the Larmor times

We calculate the characteristic Larmor times using the weak measurement formalism[13]. The projection operator onto the barrier region, Θ, has eigenvalues 1 (for particles in the barrier region) and 0 (for particles outside). A dwell time operator $D = \int_{-\infty}^{\infty} \mathrm{d}t\Theta(t)$ provides a measure of the time spent in the barrier. However, its expectation value includes contributions from both transmitted and reflected atoms. It has been shown[11,12] that the weak value of this operator, $D_w = \tau_y - i\tau_z = \langle f \mid D \mid i\rangle / \langle f \mid i\rangle$ where 'i' refers to the initial state and 'f' to the final state, can be understood as the conditional dwell time of a particle which is prepared in the $|i\rangle$ state and postselected in the $|f\rangle$ state. In our experiment, the initial state corresponds to atoms incident on the barrier from the left, and the final state corresponds to transmitted atoms on the right side of the barrier. As originally shown[15] for a square barrier, and later generalized to arbitrary potentials[44], these Larmor times can also be calculated as follows: $\tau_y = -\hbar\partial\varphi/\partial V$ and $\tau_z = -\hbar\partial \log|T|/\partial V$, where φ and $|T|$ are the phase and the magnitude of the transmission amplitude, respectively.

Using the transfer-matrix method, we numerically solve for the conditional dwell times at different incident energies. In the experiment, the Larmor probe is implemented by the pair of Raman beams; therefore, in the calculations, we obtain the dwell times by integrating over the Gaussian region of the barrier (the top-hat function Θ is replaced with a Gaussian weight function, representing the local strength of the interaction with the clock). This integration region extends beyond the turning points of the barrier for the range of incident energies, and we calculate that about 40% of the measured time for the lowest incident energy comes from the time spent in the classically forbidden region.

Spin preparation, rotation and readout

After we accelerate the atoms using a 15 G cm^{-1} magnetic gradient pulse for a variable time (0–0.9 ms), we prepare the spin state of the atoms. While the atoms travel towards the barrier, we ramp up the magnetic field to approximately 40 G. The high magnetic field causes a difference in successive energy splittings of the $F = 2$ manifold of 210 kHz as a result of the quadratic Zeeman shift. This allows us to transfer the atoms from $|2, 2\rangle$ (the state in which they Bose-condensed) to $|2, 0\rangle$, using a 1-ms radio-frequency rapid adiabatic passage. A multi-loop antenna provides the radio-frequency coupling with a Rabi frequency of approximately $\Omega_{\mathrm{rf}} \approx 2\pi \times 9$ kHz. The transfer efficiency is greater than 95%, and the atoms left behind can be identified and do not affect the subsequent dynamics in the experiment. The total preparation sequence lasts for 9 ms. Because the clock transition has a field dependence of 575 Hz G^{-2}, we lower the magnetic field to 1 G before the interaction with the Raman beams to reduce our sensitivity to magnetic noise.

For the read-out sequence, we again increase the magnetic field to 40 G. Owing to the quadratic Zeeman shift, the frequency difference between the $|1, 0\rangle$ to $|2, -1\rangle$ and the $|1, -1\rangle$ to $|2, 0\rangle$ transitions is 110 kHz. We transfer the atoms through a rapid adiabatic passage from $|1, 0\rangle$ to $|2, -1\rangle$ in 1.5 ms. The transfer efficiency is 90%. This sequence lasts for 8.5 ms.

Subsequently, we lower the magnetic field to 1 G and perform a 5.5-ms free expansion with a 40 G cm^{-1} magnetic gradient to implement a Stern–Gerlach measurement and simultaneously image both of the final states.

We can only directly measure the hyperfine states $|+x\rangle$ ($|2, 0\rangle$) and $|-x\rangle$ ($|1, 0\rangle$), thus obtaining $\langle S_x\rangle$. To complete the tomography, after the interaction with the barrier we apply a microwave pulse addressing the $|+x\rangle$ and the $|-x\rangle$ states to perform a π/2 rotation along the z axis to measure $\langle S_y\rangle$. Similarly, we rotate the spin by π/2 along the y axis, through a phase shift of π/2 radians in the driving field, to measure $\langle S_z\rangle$. The rotations are done with a dipole antenna driving the atoms with a Rabi frequency of $\Omega_{mw} = 2\pi \times 2.4$ kHz. To identify and account for possible systematic errors such as imperfect π/2 rotations or population transfer in the read-out sequence, we also measure the $-x$, $-y$ and $-z$ projections. We periodically calibrate the phase between the microwave source and the Raman beams because drifts in the ECDL frequency and changes in the etalon owing to temperature fluctuations can occur. The phase calibration is performed as follows: a spin rotation along the z axis, for atoms with an incident velocity well above the barrier height, is induced by the Raman beams and followed by a microwave pulse tuned to provide a π/2 rotation about a torque vector which lies in the y–z plane of the Bloch sphere; its angle on this plane depends on the phase of the microwave source (relative to that of the Raman beams). We repeat the procedure while scanning the phase of the microwave source and determine the phase difference from the sinusoidal behaviour of the measured hyperfine populations. For this calibration, we use a 120(7)-nK barrier and an incident velocity of 8.70(15) mm s^{-1}. The typical phase drift between calibrations is 90 mrad and has been included in the measurement uncertainties. Finally, the Larmor rotation angles[15] are found by calculating $\theta_y = \arctan(\langle S_y\rangle/\langle S_x\rangle)$ and $\theta_z = \operatorname{arctanh}\langle S_z\rangle$; although the in-plane angle arises from a phase accumulation and can thus be calculated trigonometrically, θ_z is related to the logarithmic derivative of a transmission probability, related to the inverse hyperbolic tangent of $\langle S_z\rangle$—in the limit of small Larmor frequencies, this can be equally well described by an arctangent, but in the regime of our experiment we prefer not to make the small-angle approximation, and we therefore keep the more accurate expression.

Numerical methods

Transfer-matrix method. We use the transfer-matrix method[45,46] to solve the one-dimensional Schrödinger equation. The method describes the wave after propagating by a distance δx in a potential V, $\Psi_{out} = Ae^{ikx} + Be^{-ikx}$, in terms of the incident wave, $\Psi_{in} = Ce^{ikx} + De^{-ikx}$, where $k = \sqrt{2m(E - V_0)}/\hbar$, through $\Psi_{out} = M(\delta x, V)\Psi_{in}$, where M is the so-called transfer matrix that relates the two waves. By discretizing the potential, the transmission and reflection coefficients can be calculated at any point in space.

The results of the transfer-matrix method are used to calculate the conditional dwell times, specifically the projector Θ onto the barrier region for the transmitted particles. Following the weak-value formalism[11,12], we find the projector to be

$$\langle\Theta\rangle_t = |\Psi_i(x,t)|^2 + \frac{R}{T}\Psi_i^*(-x,t)\Psi_i(x,t)$$

where the angle brackets denote the expectation value, Ψ_i and Ψ_i^* refer to the incident wave and its complex conjugate, and R and T are the reflection and transmission amplitudes, respectively. Using this projector, the Larmor-time density can be calculated (see Extended Data Fig. 1), and integrating over the barrier region yields the two characteristic times, τ_y and τ_z.

Schrödinger and Gross–Pitaevskii simulations. We solve the coupled time-dependent equations via the time-splitting spectral method[47–49]

$$i\hbar\frac{\partial\psi_1}{\partial t} = \left[-\frac{\hbar^2}{2m}\nabla^2 + V(r) + U_{11}|\psi_1|^2 + U_{12}|\psi_2|^2 + \hbar\delta\right]\psi_1 + \hbar\Omega\psi_2$$

$$i\hbar\frac{\partial\psi_2}{\partial t} = \left[-\frac{\hbar^2}{2m}\nabla^2 + V(r) + U_{21}|\psi_1|^2 + U_{22}|\psi_2|^2\right]\psi_2 + \hbar\Omega\psi_1$$

where $U_{ij} = 4\pi\hbar^2 a_{ij}/m$, a_{ij} is the s-wave scattering length between the i and j components, Ω is the Rabi frequency describing the strength of an external coupling field, and $\hbar\delta$ is an energy offset. The set of equations can be reduced from the three-dimensional to the one-dimensional case on the basis of the assumption $\omega_z \ll \omega_x, \omega_y$ where ω_x and ω_y are the trap frequencies along the axes that are orthogonal to z. This criterion is met in our experiment, as $\omega_z = 2\pi \times 2.7$ Hz and $\omega_{x,y} = 2\pi \times 220$ Hz. The ground state of the trap is found by imaginary time propagation. Initially, a constant energy offset is added to one of the components during this evolution to favour the ground state of the trap for only one of the spin components. The atoms are released from the initial potential, and a phase gradient is written across the wavepacket to set the velocity and launch it against the barrier. In the barrier region, coupling between the two components—with the same Gaussian profile of the barrier—is implemented to simulate the Raman coupling. The total duration of the simulations is set such that all the atoms have finished interacting with the barrier. By setting the scattering lengths to zero, we go from the Gross–Pitaevskii equation, also known as the nonlinear Schrödinger equation, to the Schrödinger equation. We find no major differences between the interacting and the non-interacting cases (see Extended Data Fig. 2).

Data availability

The data presented in the figures and that support the other findings of this study are available from the corresponding author on reasonable request. Source data are provided with this paper.

38. Chu, S., Bjorkholm, J. E., Ashkin, A., Gordon, J. P. & Hollberg, L. W. Proposal for optically cooling atoms to temperatures of the order of 10^{-6} K. *Opt. Lett.* **11**, 73–75 (1986).
39. Ammann, H. & Christensen, N. Delta-kick cooling: a new method for cooling atoms. *Phys. Rev. Lett.* **78**, 2088–2091 (1997).
40. Morinaga, M., Bouchoule, I., Karam, J.-C. & Salomon, C. Manipulation of motional quantum states of neutral atoms. *Phys. Rev. Lett.* **83**, 4037–4040 (1999).
41. Maréchal, E. et al. Longitudinal focusing of an atomic cloud using pulsed magnetic forces. *Phys. Rev. A* **59**, 4636–4640 (1999).
42. Myrskog, S. H., Fox, J. K., Moon, H. S., Kim, J. B. & Steinberg, A. M. Modified "delta -kick cooling" using magnetic field gradients. *Phys. Rev. A* **61**, 053412 (2000).
43. Le Kien, F., Schneeweiss, P. & Rauschenbeutel, A. Dynamical polarizability of atoms in arbitrary light fields: general theory and application to cesium. *Eur. Phys. J. D* **67**, 92 (2013).
44. Leavens, C. R. & Aers, G. C. Extension to arbitrary barrier of the Büttiker–Landauer characteristic barrier interaction times. *Solid State Commun.* **63**, 1101–1105 (1987).
45. Cohen-Tannoudji, C., Diu, B. & Laloë, F. *Quantum Mechanics* (Wiley, 1977).
46. Sánchez-Soto, L. L., Monzón, J. J., Barriuso, A. G. & Cariñena, J. F. The transfer matrix: a geometrical perspective. *Phys. Rep.* **513**, 191–227 (2013).
47. Bao, W. & Cai, Y. Mathematical theory and numerical methods for Bose–Einstein condensation. *Kinetic Relat. Models* **6**, 1–135 (2012).
48. Wang, H. A time-splitting spectral method for computing dynamics of spinor $F = 1$ Bose–Einstein condensates. *Int. J. Comput. Math.* **84**, 925–944 (2007).
49. Bao, W. Ground states and dynamics of multicomponent Bose–Einstein condensates. *Multiscale Model. Sim.* **2**, 210–236 (2004).

Acknowledgements We acknowledge years of hard work by the people who created the Bose–Einstein condensation apparatus and helped make the present experiment possible: A. Jofre, M. Siercke, C. Ellenor, M. Martinelli, R. Chang, S. Potnis and A. Stummer. We thank J. Thywissen, A. Vutha, J. McGowan, K. Bonsma-Fisher and A. Brodutch for discussions. This work was supported by NSERC and the Fetzer Franklin Fund of the John E. Fetzer Memorial Trust. A.M.S. is a fellow of CIFAR. R.R. acknowledges support from CONACYT.

Author contributions R.R., D.S. and I.R. performed the experiments. A.M.S. supervised the work. All authors made contributions to the work, discussed the results and contributed to the writing of the manuscript.

Competing interests The authors declare no competing interests.

Additional information
Correspondence and requests for materials should be addressed to R.R.
Peer review information *Nature* thanks Adolfo Del Campo, Olga Smirnova and the other, anonymous, reviewer(s) for their contribution to the peer review of this work.
Reprints and permissions information is available at http://www.nature.com/reprints.

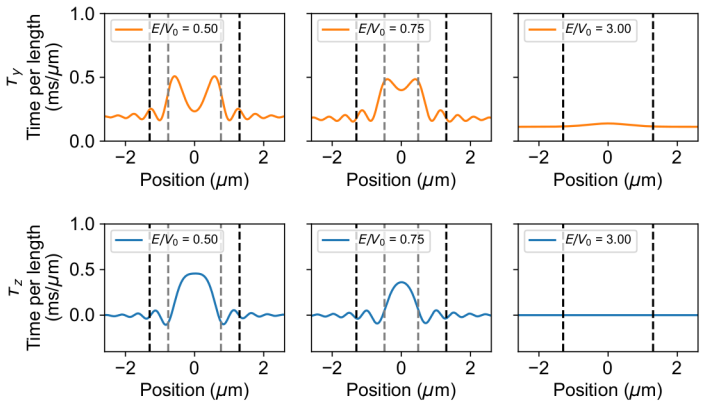

Extended Data Fig. 1 | Calculated time density of the Larmor components τ_y and τ_z using the transfer-matrix method for a 135-nK Gaussian barrier. The black dashed lines indicate the $1/e^2$ radius of the Gaussian barrier and the grey lines show the classical turning points. The Larmor time τ_y (or τ_z) is obtained by integrating over space, taking into account the position-dependent coupling of the Raman beams.

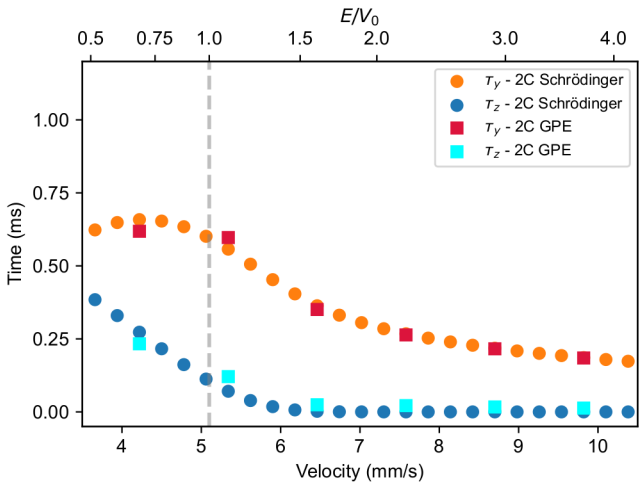

Extended Data Fig. 2 | Simulations of the Larmor clock. The simulations correspond to one-dimensional two-component time-dependent Schrödinger and Gross–Pitaevskii simulations. The parameters are as in Fig. 4.